NJC

PAPER

View Article Online
View Journal | View Issue

Cite this: *New J. Chem.*, 2014, **38**, 1106

PEDOT nanostructures synthesized in hexagonal mesophases†

Srabanti Ghosh,[a] Hynd Remita,[a] Laurence Ramos,[bc] Alexandre Dazzi,[a] Ariane Deniset-Besseau,[a] Patricia Beaunier,[d] Fabrice Goubard,[e] Pierre-Henri Aubert,[e] Francois Brisset[f] and Samy Remita*[ag]

Received (in Montpellier, France) 31st October 2013,
Accepted 28th December 2013

DOI: 10.1039/c3nj01349a

www.rsc.org/njc

We describe a single step preparation of nanostructures of poly(3,4-ethylenedioxythiophene), PEDOT, in the hydrophobic domains of cationic surfactant-based hexagonal mesophases *via* chemical oxidative polymerization of EDOT monomers using $FeCl_3$ as an oxidizing agent. After polymerization, the hexagonal structure of the mesophases is preserved as demonstrated by polarized light microscopy and X-ray scattering measurements. After extraction from mesophases, the chemical structure of PEDOT is confirmed by Fourier transform infrared spectroscopy. Moreover, PEDOT morphology is checked by transmission and scanning electron microscopies. PEDOT nanostructures with spindle-like or vesicle-like shapes are obtained depending on the experimental conditions. In the original method, high resolution atomic force microscopy, coupled with infrared nanospectroscopy, is used to probe the local chemical composition of PEDOT nanostructures. Finally, the as-prepared PEDOT polymers are characterized by both good thermal stability up to 200 °C and a relatively high conductivity value up to 0.4 S cm^{-1} as determined by thermogravimetric analysis and four probe measurements respectively.

Introduction

The development of new synthetic methodologies with an emphasis on rational control of morphology and size of nano-scale materials can facilitate revolutionary advances in science and technology.[1,2] In this context, conjugated polymers have been the subject of intense research due to the combination of superior optoelectronic properties of semiconductors (such as high conductivity, mechanical and thermal stability) along with the advantages of organic materials (low cost, easy processing and enormous opportunities intended for structural modification).[3,4] Recent progress established that conjugated polymers deliver great strides as active elements in electronic and optoelectronic devices as light emitting diodes for display applications, thin film transistors for low-cost and ultra-dense logic and memory circuits, photodiodes for optical information processing, photovoltaic cells for solar energy harvesting, sensors and biomedical applications.[5–8]

Among π-conjugated polymers, poly(3,4-ethylenedioxythiophene) (PEDOT) (Scheme 1) is one of the most promising conducting systems, having excellent environmental stability and high electrical conductivity,[9–11] which makes it an ideal candidate for various applications such as electronic, optical, and electrochemical applications.[12–14] Generally, polymerization of 3,4-ethylenedioxythiophene (EDOT) (Scheme 1) monomers, which leads to PEDOT, is based on a variety of protocols, such as wet chemical oxidation in particular by iron salts, interfacial polymerization, electrochemical polymerization or vapor phase polymerization.[15–17]

There has been wide spread interest in the fabrication of different organic micro/nano structures with specific morphologies in a cost-effective way. Besides, significant efforts are underway to explore new techniques intended for tailoring the polymer size and

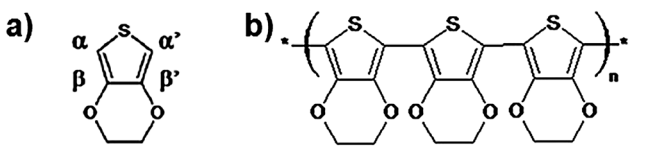

Scheme 1 Chemical structures of EDOT monomer (a) and PEDOT polymer (b). The free α and α′ positions of EDOT monomers are involved during polymerization.

[a] *Laboratoire de Chimie Physique, UMR 8000-CNRS, Bât. 349, Université Paris-Sud, 91405 Orsay, France. E-mail: samy.remita@u-psud.fr*
[b] *Laboratoire Charles Coulomb UMR 5221, Université Montpellier 2, F-34095, Montpellier, France*
[c] *Laboratoire Charles Coulomb UMR 5221, CNRS, F-34095, Montpellier, France*
[d] *Laboratoire de Réactivité de Surface, UMR 7197-CNRS, UPMC, Université Paris 6, 75006 Paris, France*
[e] *Laboratoire de Physicochimie des Polymères et Interfaces (LPPI), Université de Cergy-Pontoise, 95031 Cergy-Pontoise Cedex, France*
[f] *ICMMO, UMR 8182-CNRS, Bât. 410-420, Université Paris-Sud, 91405 Orsay, France*
[g] *Département CASER, Ecole SITI, Conservatoire National des Arts et Métiers, CNAM, 292 rue Saint-Martin, 75141 Paris Cedex 03, France*

† Electronic supplementary information (ESI) available. See DOI: 10.1039/c3nj01349a

shape, which in turn improve their optoelectronic properties.[18–21] Importantly, a variety of lyotropic liquid crystals (LCs) including hexagonal or lamellar phases have been employed for the high degree of orientational order of conducting polymers with anisotropic morphologies, which cannot be achieved using traditional bulk or solution polymerizations.[22,23] Nevertheless, in the particular case of PEDOT, there are only very few reports which concern the fabrication of nanostructures within LC templates.[24–26] In these rare cases, the electropolymerization technique was used and enabled, for instance, the fabrication of hexagonally ordered fibrillar PEDOT nanostructures into hexagonal LCs.[25,27]

In the past few years, we have employed swollen hexagonal mesophases as versatile soft templates doped with various compounds to synthesize different nanostructured materials (such as metals, polymers or oxides) in both aqueous and oil phases.[28–30] The mesophases composed of oil-swollen tubes with tunable diameters,[31,32] which are stabilized by a monolayer of surfactant and cosurfactant molecules, have been shown to effectively control and modulate the morphology and the size of the nanostructures.[33–35] Moreover, controlling the liquid-crystalline phase, depending on composition ranging from hexagonal to lamellar or cubic phases, can direct the dimensionality and the morphology of the nanoobjects grown *in situ*.[36,37] In addition to structure directing ability, the swollen hexagonal mesophases present interesting characteristics in terms of environmental safety and cost. Hence, it would be interesting to explore hexagonal mesophase assisted fabrication of conducting polymer nanostructures in particular *via* a chemical oxidative process. Moreover, for a facile one pot strategy and large-scale approach, it is imperative to seek the preparation of polymer nanostructures in a controlled fashion.

In the present study, we use cationic surfactant based hexagonal mesophases as templates for the preparation of PEDOT nanostructures in a simple chemical route. The idea is first to dope the mesophases with both EDOT, as a monomer, and an iron salt, as oxidizing species, to initiate PEDOT polymerization, and second to use the architecture of the mesophases and their hydrophilic/hydrophobic properties in order to control the morphology of the nanostructures.

Experimental section

Materials

3,4-Ethylenedioxythiophene (EDOT), as a monomer, iron(III) chloride, as an oxidative agent, cetyltrimethylammonium bromide (CTAB) ($\geq$98%), sodium chloride, toluene (>99%) and pentanol ($\geq$99%), for hexagonal mesophase preparation, were all purchased from Sigma-Aldrich. Ultrapure water (Millipore System, 18.2 MΩ cm) and ethanol ($\geq$99% for HPLC, purchased from Sigma-Aldrich) were used as solvents, in particular for PEDOT extraction from hexagonal mesophases.

Synthetic methodology for PEDOT preparation

The hexagonal mesophases were made of a mixture of cetyltrimethylammonium bromide (CTAB) as a surfactant, salt water (NaCl), toluene as oil and pentanol as a cosurfactant. In a typical preparation of swollen hexagonal mesophases, 1.03 g of CTAB was dissolved in 2 mL of an aqueous solution containing salt (0.1 M NaCl). After vigorous agitation for few minutes at 50 °C, the surfactant (CTAB) was completely dissolved giving a transparent and viscous micellar solution. The subsequent addition of 2.98 mL of toluene in the micellar solution under stirring induced the formation of a white unstable emulsion. The cosurfactant (20 μL of pentanol) was then added to the mixture which was strongly vortexed for a few minutes. This led to a perfectly translucent, birefringent and stable gel consisting of a hexagonal mesophase. This system exhibits oil in water (O/W) direct phase structure made of hexagonally packed nonpolar cylinders filled by toluene and stabilized by a monolayer of cationic surfactants and cosurfactants that can be surrounded by a continuous water domain.[28,31,32]

According to the same procedure, other mesophases were also prepared in the presence of EDOT alone, in the presence of $FeCl_3$ alone or in the presence of both EDOT and $FeCl_3$ (always in the same proportions). EDOT and/or $FeCl_3$ were dissolved separately in toluene and added to the viscous micellar solution during mesophase preparation. Evidently, EDOT and $FeCl_3$ were never mixed together before this step in order to avoid bulk polymerization. Additionally, the swelling of the mesophases was varied by changing the volume ratio of oil over water (O/W). We varied both O/W ratio and NaCl concentration simultaneously. For example, mesophases with O/W = 1.5 and NaCl at 0.1 M or with O/W = 2.5 and NaCl at 0.3 M were prepared at fixed EDOT concentrations.

We checked, by UV-vis absorption spectrophotometry, that EDOT is soluble within the organic phase of mesophases up to 0.3 M. Since EDOT is only sparingly soluble in water ($<$0.002 M),[25] we conclude that EDOT is mainly present in the hydrophobic regions of the hexagonal LC (into toluene phase). One can then predict that EDOT polymerization can only be initiated in the hydrophobic region of swollen hexagonal mesophases. Moreover, since PEDOT oligomers and polymers present poor hydrophilic properties, one can also imagine that polymer growth can take place only in toluene.

While EDOT-containing mesophases remain colorless, hexagonal mesophases containing the $FeCl_3$ salt have a yellow color (Fig. S1, ESI†) due to the absorption of Fe^{3+} ions (Fig. S2, ESI†). The simultaneous presence of EDOT and $FeCl_3$ in the mesophases induces a rapid change in the coloration of the systems: the initial yellow gel quickly turns into a dark blue gel which, nevertheless, remains translucent (Fig. S1, ESI†). This change in color indicates a chemical transformation which occurs within the mesophases and which will further be attributed to iron-induced EDOT polymerization.

In order to extract PEDOT polymers from the mesophases and for further characterization, the hexagonal mesophases were destabilized by the addition of equal volumes of ethanol and water. Note that ethanol, which is less polar than water, is not only used here for mesophase destabilization, but also for enabling dissolution and dispersion of PEDOT polymers. With this protocol, a complete phase separation occurs with the

organic portion in the upper phase (ethanolic phase) containing a black matter which will be identified as PEDOT. The mixture was then centrifuged and the extracted blue powder was washed with ethanol several times to remove unused reactants such as monomers and oxidants. The PEDOT was then recovered as a pure solid after full evaporation of the organic phase and was eventually redispersed in ethanol when using solution characterization techniques. The purity of the solid PEDOT and thus the validity of the extraction procedure were both evaluated by the measurement of the solid powder melting point.

In order to check the influence of the presence of mesophases onto the growth and then onto the final morphology of synthesized polymers, PEDOT was also synthesized in bulk solution by mixing EDOT and $FeCl_3$ in the same proportions in toluene solvent (without using mesophases). The black powder obtained immediately after mixing EDOT with $FeCl_3$ was washed several times with ethanol and was characterized for comparison. Additionally, in order to check whether mesophases can *a posteriori* affect the morphology of soft materials such as PEDOT, these bulk polymers were mixed with pure mesophases (prepared in the absence of EDOT and $FeCl_3$) and then extracted using equal volumes of ethanol and water as mentioned above.

Material characterization

The pure mesophases containing gels and the mesophases doped with EDOT monomers and/or with $FeCl_3$ were analyzed by small-angle X-ray scattering (SAXS) both before and after the color change of the gel. The mesophases were inserted in glass capillaries of 1.5 mm diameter and a high brightness low power X-ray tube, coupled with an aspheric multilayer optic (GeniX 3D from Xenocs) was employed, which delivered an ultralow divergent beam (0.5 mrad). Scatterless slits were used to give a clean 0.8 mm diameter X-ray spot with an estimated flux around 35 mph s^{-1} at the sample position. A transmission configuration was used. The scattered intensity was collected on a two-dimensional Schneider 2D image plate detector prototype, at a distance of 1.9 m from the sample. The experimental data were corrected for the background scattering and the sample transmission. The scattering vector q can be calculated from the angle of the scattered radiation and the X-ray wavelength.

Optical microscopy of gel samples before and after polymerization was performed using a Leica DMRX polarizing microscope. Additionally, the as-prepared pure and doped (with both EDOT and $FeCl_3$) hexagonal mesophases were observed by transmission electron microscopy in a cryogenic environment (Cryo-TEM) using an ultrascan 2kCCD camera (Gatan, USA), and a LaB6 JEOL JEM 2100 (JEOL, Japan) cryomicroscope operating at 200 kV. The Cryo-TEM, ensures the observation of soft nano-objects in equilibrium *via* a freezing process avoiding the phase transition and the possible particle aggregation which should result from drying procedures. A small amount of gel samples ($\sim$20 μL) was deposited on "quantifoil"® (Quantifoil Micro Tools GmbH, Germany) 200 mesh hole-carbon coated grids. After being blotted with a filter paper, the grids were quench-frozen by being rapidly plunged into liquid ethane in order to form a thin ice film avoiding water crystallization. The grids were then transferred into the microscope using a side entry Gatan 626 cryo holder cooled at −180 °C with liquid nitrogen.

For chemical identification of PEDOT, attenuated total reflectance Fourier transform infrared (ATR-FTIR) spectroscopy was used. ATR-FTIR spectra of pure EDOT monomers, of solid PEDOT powders prepared in bulk solution, or of PEDOT powders obtained after extraction from the mesophases were recorded using a Bruker Vertex 70 FTIR spectrometer with diamond ATR attachment (PIKEMIRACLE crystal plated diamond/ZnSe) and a mercury–cadmium–telluride (MCT) detector with a liquid nitrogen cooling system. Scanning wavelengths were varied from 4000 to 600 cm^{-1} with a 4 cm^{-1} spectral resolution using 100 repetition scans on average for each spectrum.

Thermal stability analysis of the PEDOT powders prepared in bulk solution or obtained after extraction from the mesophases was carried out by using a TGA DQ_{50} thermogravimetric analysis (TGA) apparatus (TA instruments, USA). The test was carried out in air with a heating rate of 20 °C min^{-1} from 50 °C to 600 °C, the samples were then isothermally treated for 30 min at 600 °C. Differential scanning calorimetry traces were obtained using a TA Instruments Q100 DSC, using indium as the calibration standard, with a heating or cooling rate of 10 °C min^{-1} under a nitrogen atmosphere.

UV-visible absorption spectra of ethanolic solutions containing pure EDOT, $FeCl_3$ salt or dissolved PEDOT powder after extraction from mesophases were recorded using a HP8543 spectrophotometer. Ethanol solvent was always taken as reference.

The morphology eventually combined with the local IR spectrum of synthesized PEDOT deposited onto the solid substrate was determined by combining the classical atomic force microscopy (AFM) with free-electron laser as the IR source (AFM-IR). The AFM-IR technique combines an atomic force microscope with a pulsed infrared laser to perform spectromicroscopy beyond the conventional optical diffraction limit. We used a commercially available AFM (Veeco Explorer model), which has a visible laser focused on the cantilever, and a four quadrant detector measuring its deflection using a bench top tunable laser source.[38–40] For the present study, we used a commercial setup, nano-IR (Anasys Instrument corp.) allowing us to cover the spectral range from 3600 cm^{-1} to 1000 cm^{-1}. Usually, samples are directly deposited on the upper surface of a ZnSe prism that is transparent in the mid-infrared and the tip of the AFM remains in contact with the object. When the sample absorbs the IR laser pulse, it warms *via* the photothermal effect resulting in a rapid thermal expansion of the absorbing region of the sample. The thermal expansion pulse impacts the tip of the AFM cantilever and causes its oscillation. As the amplitude of oscillations is proportional to the absorption, we are able to record infrared absorption spectra at a given point and to make chemical maps by scanning the surface at a given wavelength.[41] For chemical mapping, the laser wave number is fixed at a value corresponding to a specific absorption band characterizing a functional group and the tip is scanned over the sample. In this study, drops of ethanolic solutions of PEDOT powder after extraction from the mesophases were

directly deposited on the upper surface of a ZnSe prism and dried at room temperature.

For further structural study of PEDOT polymers, drops of the PEDOT ethanolic solutions after extraction from mesophases were also deposited on carbon coated grids. Transmission electron microscope (TEM) observations were performed on a JEOL JEM 100 CXII transmission electron microscope at an accelerating voltage of 100 kV. The images were collected using a 4008 × 2672 pixels CCD camera (Gatan Orius SC1000).

The morphology of the PEDOT nanostructures after extraction from the mesophases was also observed using a high resolution scanning electron microscope Zeiss Supra 55 FEG-SEM. In this case, drops of PEDOT ethanolic solutions, after extraction from mesophases, were deposited on aluminium substrates.

Finally, spin-coated films were fabricated on glass slides at 1000 rpm for 60s using the PEDOT ethanolic solutions obtained after extraction from mesophases. In addition, PEDOT nanostructures obtained after extraction from mesophases were treated with $NOBF_4$, a chemical oxidant, at a concentration of 10^{-2} M in acetonitrile and were then spin-coated under the same conditions. The thickness (*ca.* 200–500 nm thickness) of all the films (doped or non-doped) was measured using a 3 Veeco Dektak 150 surface profiler. The electrical conductivity of the polymer films was measured using a Kelvin four-point probe technique implemented with a Keithley 2420 system. The conductivity, ρ (S cm^{-1}) was determined using the following equation:

$$\rho = \left(\frac{\pi}{\ln(2)} \times \frac{V}{I} \times t\right)^{-1}$$

where V is the voltage difference (V), t the film thickness (cm) and I the applied current (A).

Results and discussion

PEDOT synthesis in mesophases

Swollen hexagonal mesophases, resulting from the surfactant mediated self-assembly in a quaternary system (water, surfactant, cosurfactant, and oil), serve as versatile templates for synthesizing various nanomaterials.[28–35,42] For PEDOT synthesis, we prepared pure mesophases at 0.1 M NaCl with a volume ratio of oil over water (O/W) (v/v) fixed at 1.5. Mesophases with similar compositions were also prepared in the presence of EDOT at varied concentrations from 0.05 to 0.3 M. All mesophases doped with EDOT monomers up to 0.3 M remained perfectly transparent and birefringent stable gels (Fig. S1, ESI†).

The swollen hexagonal phases doped with increasing EDOT concentrations were studied by small angle X-ray scattering (SAXS) and appeared as representative hexagonal LC mesophases as shown in Fig. 1a. The hexagonal symmetry of the mesophases can be unambiguously identified by the occurrence of three Bragg peaks in the scattered intensity, whose positions are in the ratio of $1:\sqrt{3}:2$. In all cases, three Bragg peaks with relative positions expected for a hexagonal phase were found to have a similar lattice parameter of 19.1 ± 0.5 nm

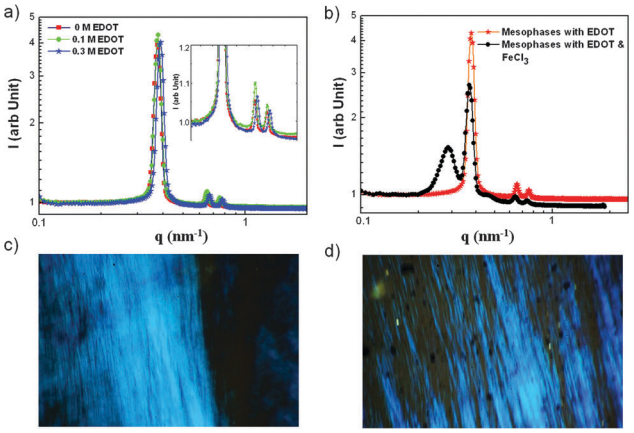

Fig. 1 SAXS spectra of hexagonal mesophases at 0.1 M NaCl with increasing EDOT concentrations (0 M, 0.1 M and 0.3 M) (a); SAXS spectra of hexagonal mesophases at 0.1 M NaCl in the presence of 0.1 M EDOT with or without $FeCl_3$ (0.1 M) (b); polarized light micrograph of mesophases in the absence of EDOT and $FeCl_3$ (c); polarized light micrograph of doped mesophases with both 0.1 M EDOT and 0.1 M $FeCl_3$ (d).

in the absence or in the presence of EDOT monomers. This result suggests that swollen hexagonal mesophases can be used as stable soft templates providing confining media for the oxidative polymerization of EDOT. The presence of $FeCl_3$ (0.1 M) as a chemical oxidant in the mesophases also led to yellow perfectly transparent and birefringent stable gels (Fig. S1, ESI†). Note that the observed yellow coloration is due to the absorption properties of $FeCl_3$ (Fig. S2, ESI†). This result also suggests that the incorporation of the iron chloride salt does not destabilize the mesophases.

In the presence of EDOT monomers and the $FeCl_3$ chemical oxidant together (in the same proportion), the mesophases turned in all cases into a translucent birefringent dark blue gel in a few minutes (Fig. S1, ESI†). This color change indicates that a chemical reaction took place within the mesophases, which will be further attributed to PEDOT synthesis *via* oxidation of EDOT by $FeCl_3$. Nevertheless, at this stage of the work, the attribution of the dark blue color to PEDOT polymers trapped into the mesophases is conceivable since this color is that generally observed in the literature for PEDOT polymers.[25]

The stability of the mesophases doped with both EDOT (at 0.1 M) and $FeCl_3$ (at 0.1 M) was also checked by SAXS measurements (Fig. 1b). The X-ray scattering profile displays three Bragg peaks, the positions of which are in the ratio $1:\sqrt{3}:2$. One can note that these three peaks are not displaced in comparison with those obtained in the absence of iron chloride (Fig. 1a). This demonstrates that the hexagonal structure of the gels is preserved. Similar observations were obtained when varying the experimental conditions (concentrations of both monomers and iron salts on one hand, or NaCl concentration on the other hand) indicating that whatever our experimental conditions, a relatively large degree of liquid crystalline order was preserved when mixing EDOT and $FeCl_3$ in the oil phase of the mesophases. Nevertheless, in addition to the three previous peaks, an additional broad peak is observed in all

cases at around 0.288 nm^{-1}. Even if the origin of this peak is still not understood, its presence reveals the occurrence of a chemical transformation within the mesophases.

The hexagonal phases are birefringent and exhibit characteristic textures between crossed polarizing windows when the surfactant cylinders are parallel to the walls of the observation cell. The polarized optical microscopy (Fig. 1c and d) demonstrates that the presence of EDOT and iron chloride does not affect the birefringent nature of the gels or their texture as expected for hexagonal mesophases. However, dark spots can be observed in the presence of both EDOT and $FeCl_3$ (Fig. 1d). This could be due to the presence of new compounds produced by the reaction of EDOT with $FeCl_3$ in the mesophase.

The hexagonal mesophases were also observed by cryo-TEM microscopy. Tube rod-like micelles were clearly observed in all cases, even in the presence of EDOT and $FeCl_3$ (Fig. S3, ESI†), as expected for hexagonal mesophases. These observations are obviously in very good agreement with SAXS measurements.

In order to identify the chemical nature of the products, which are responsible for the dark blue coloration of the gels, and in order to perform morphological characterizations, the synthesized products were extracted from the mesophases.

PEDOT identification

The chemical structure of the dark blue powder extracted from mesophases was first characterized by using ATR-Fourier transform infrared spectroscopy (FTIR). The ATR-FTIR spectrum of the product formed in the mesophases in the presence of both EDOT and $FeCl_3$ (both at 0.1 M) was compared with those of pure EDOT monomers and of PEDOT solid powder synthesized in bulk solutions in the absence of mesophases (Fig. 2). One can note that even if the absorption bands are slightly shifted, the FTIR spectrum of the product obtained in mesophases (Spectrum 2b) is similar to that of PEDOT we synthesized in bulk solution (Spectrum 2c). These two spectra are also in good agreement with the spectrum of PEDOT obtained in the literature.[43]

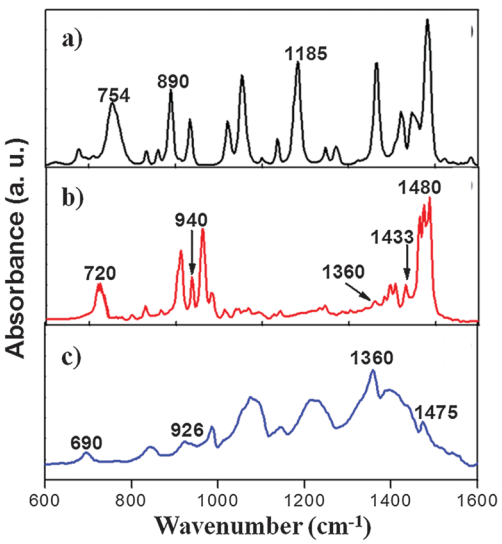

Fig. 2 ATR-FTIR spectra of EDOT monomers (a), PEDOT synthesized in hexagonal mesophases at 0.1 M NaCl with EDOT (0.1 M) and $FeCl_3$ (0.1 M) (b) and PEDOT synthesized in bulk solution (c).

In addition, the C–H stretching band at 754 cm^{-1} observed in the EDOT spectrum is not present in spectra 2b and 2c. This clearly indicates EDOT polymerization, thanks to α–α′ coupling, and suggests PEDOT formation not only in the bulk but also into the mesophases.[44] The other vibration bands at 1480, 1433 and 1360 cm^{-1} in spectrum 2b are due to stretching modes of C=C and C–C originating from the thiophene ring, while the bands at 1299, 1243, 1141 and 1068 cm^{-1} correspond to C–O–C bond stretching in the ethylene oxide group (Scheme 1). Bands at 940, 902 and 826 cm^{-1} are those of the C–S bond in the thiophene ring. Note that the band at 690 cm^{-1} observed in spectrum 2c, which is related to the defects in polymer chains, is not present in the spectrum 2b of PEDOT in mesophases.

These results suggest the formation of PEDOT conjugated polymers within the confined medium of mesophases as a result of the oxidation of EDOT monomers by the iron salt. Besides, the melting point of the dark blue solid product obtained after extraction from mesophases was found to be 148 °C, which is in very good agreement with the melting point values already reported for PEDOT in the literature.[20] This definitely proves the formation of PEDOT and highlights its purity, demonstrating the validity and the efficiency of our extraction procedure. Moreover, the bands at 1185 and 890 cm^{-1} attributed to the =C–H in-plane and out-of-plane deformation vibrations of pure EDOT (Spectrum 2a) are not observed in the spectrum of PEDOT synthesized in mesophases (Spectrum 2b), nor in that of bulk PEDOT (Spectrum 2c), indicating that, under our experimental conditions, all EDOT molecules have disappeared. This could be due either to quantitative polymerization or to efficient extraction. Note that, when varying the experimental conditions (concentrations of both monomers and iron salts on one hand, or NaCl concentration on the other hand), the PEDOT nature as well as the purity of the solid powder obtained, after extraction, were always demonstrated.

After ATR-FTIR characterization, the PEDOT solid powder extracted from mesophases was dissolved in ethanol. The UV-visible absorption spectra of the PEDOT polymers synthesized at different EDOT, $FeCl_3$ and NaCl concentrations were then recorded as shown in Fig. 3 in the case of 0.1 M in both EDOT and $FeCl_3$. The absorption spectrum of Fig. 3 displays an absorption peak with a maximum at 390 nm together with a broad absorption band in the near IR-region of the spectrum. Such a spectrum is consistent with earlier studies concerning PEDOT.[45] Note that the near IR-region absorption band is related to bipolaron subgap transitions indicating a high level of doping in the polymers.[46,47]

We can note that no absorption of EDOT is observed at 215 nm and 243 nm (compared with the inset of Fig. 3). This, once again, indicates the total elimination of EDOT molecules after polymerization and the extraction procedure.

PEDOT structural characterization

Drops of ethanolic solutions containing dissolved PEDOT powder were deposited on the upper surface of a ZnSe prism then dried at

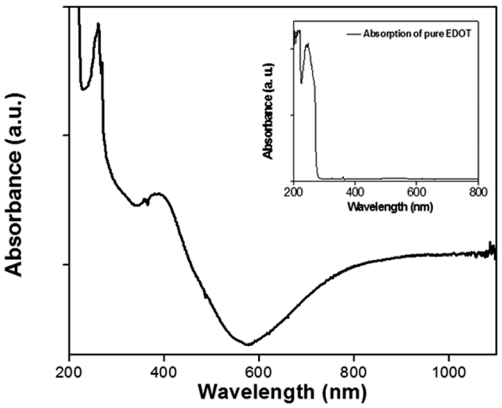

Fig. 3 UV-visible absorption spectrum of an ethanolic solution of PEDOT synthesized in mesophases at 0.1 M NaCl, 0.1 M EDOT and 0.1 M $FeCl_3$. Inset: absorption spectrum of pure EDOT monomers (0.1 M) in ethanol. The absorbances are in arbitrary units.

room temperature before AFM-IR characterization. By taking advantage of the AFM-IR technique, it is possible to obtain AFM images together with infrared spectroscopy analysis: a local infrared spectrum recorded through the change in the wavenumber of the laser.[48,49] Fig. 4a shows the AFM-IR spectrum of PEDOT formed in mesophases (at 0.1 M NaCl in the presence of both EDOT and $FeCl_3$ at 0.1 M) and deposited onto the ZnSe substrate. This AFM-IR spectrum, displayed in the 1200–1600 cm^{-1} region, is quite similar to the FTIR spectrum of PEDOT observed in Fig. 2.

The peaks at around 1360 and 1476 cm^{-1}, due to C–C and C=C stretching of the quinoïdal structure of the thiophene ring, indicate the effective presence of PEDOT.[50] Note that the band at 1334 cm^{-1} is relatively larger than that observed in the ATR-FTIR spectrum of PEDOT (Fig. 2). This difference probably comes from the water vapor absorption which still remains during the AFM-IR measurements.

The AFM-IR technique also enables the chemical mapping of the sample. Fig. 4b shows the IR absorption strength as measured by cantilever oscillations when the laser is set at 1476 cm^{-1}, while Fig. 4c displays the corresponding topography. The brighter colors indicate regions of stronger IR absorption at this particular wavenumber and hence represent objects containing PEDOT polymer molecules. Looking at the corresponding topography, we notice that the brighter regions in the absorption image correspond to the thicker region of the polymer. As the signal of absorption fits well with the thickness, we can assume that the objects deposited on the prism surface are only made of PEDOT. Further, we checked that if the tip is placed on the substrate without PEDOT, there is no signal.

The AFM-IR technique was not only used to check the structural nature of the polymers but was also performed to provide morphological characterization of PEDOT nanostructures synthesized within mesophases. The optical images of the PEDOT polymers revealed in all the cases the presence of two types of structures: (i) well dispersed isolated ones and (ii) twisted and balled-up objects which could be the result of an aggregation (Fig. S4a and b, ESI†). The first objects were easily observed and characterized by AFM, while the second structures were too soft and unstable at the tip making impossible their study by AFM. Note that the twisted and balled-up objects are predominant at 0.1 M NaCl (Fig. S4a, ESI†) while the isolated structures are predominant at 0.3 M NaCl (Fig. S4b, ESI†) whatever EDOT and $FeCl_3$ concentrations be (EDOT and $FeCl_3$ being always in the same proportions).

The isolated structures deposited onto the ZnSe substrate were observed in surface topography images of Fig. 5. These images were obtained in the case of PEDOT polymers synthesized in

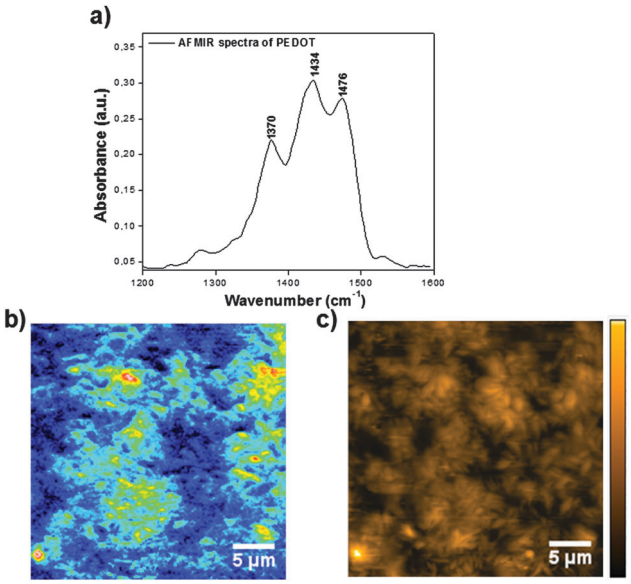

Fig. 4 AFM-IR spectrum of PEDOT synthesized in the mesophases at 0.1 M NaCl, 0.1 M EDOT and 0.1 M $FeCl_3$ (a), AFM-IR chemical map of PEDOT with the IR source tuned to the C=C band at 1476 cm^{-1} (b) and the corresponding topographic image of the PEDOT polymer (c).

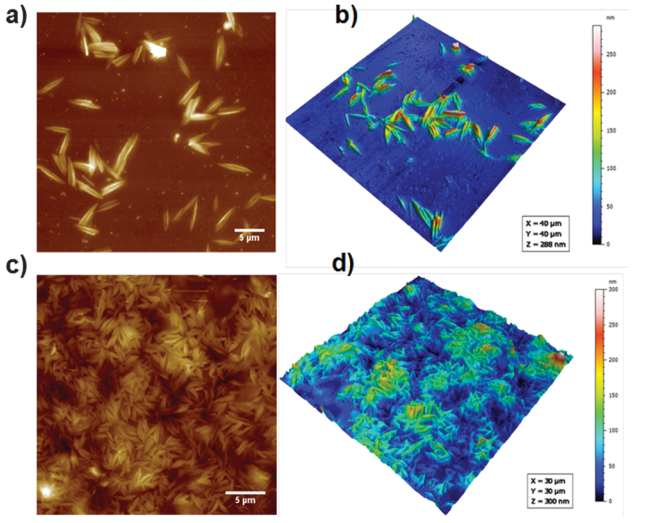

Fig. 5 AFM topographic images of PEDOT extracted from mesophases and deposited onto the ZnSe substrate. PEDOT synthesized using 0.1 M EDOT and 0.1 M $FeCl_3$ at 0.1 M NaCl (a) with the corresponding 3D AFM image (b). PEDOT synthesized using 0.1 M EDOT and 0.1 M $FeCl_3$ at 0.3 M NaCl (c) with the corresponding 3D AFM image (d).

mesophases in the presence of both EDOT and $FeCl_3$ (at 0.1 M) at two different NaCl concentrations (0.1 M or 0.3 M). The nanostructures obtained at 0.1 M NaCl appear elongated with an average spindle size around 4–6 μm (Fig. 5a). These nanoobjects seem to be flattened with a height of 70 nm as observed in the 3D AFM image (Fig. 5b). Each nanostructure which remains stable at the tip should correspond to a self assembly of PEDOT polymers which interact all together, thanks to π-stacking interactions.

In order to check whether the experimental conditions affect the morphology of PEDOT nanostructures, we varied different experimental parameters. While EDOT and $FeCl_3$ concentrations (up to 0.3 M) seem to have no influence, the increase in NaCl concentration from 0.1 M to 0.3 M leads to spindle shaped PEDOT objects with a smaller length. In the case of PEDOT polymers synthesized in mesophases at 0.3 M NaCl (instead of 0.1 M) in the presence of both EDOT and $FeCl_3$ (at 0.1 M), one can note that the length of the nanostructures is about 2 μm (Fig. 5c and d). In addition, in comparison with the images obtained at lower NaCl concentration (Fig. 5a and b), more PEDOT nanostructures with more regular shape are observed on the substrate (Fig. 5c, in comparison with Fig. 5a). Evidently, the observed difference in the number of nanostructures onto the substrate could result from the deposition procedure and from the surface coverage. However, the variation in size of the nanostructures could be due to the difference in the length of the PEDOT polymer chains when synthesized at different NaCl concentrations. Polymers may be longer when synthesized in mesophases at 0.3 M NaCl. Probably, at higher NaCl concentrations, the diffusion of EDOT and $FeCl_3$ outside the micelles is slower leading to faster polymerization which evidently should lead to a higher number of polymers with smaller sizes and more regular shapes. Eventually, at higher salt concentrations, the higher ionic strength outside the micelles could also increase the concentration of EDOT in the hydrophobic region of the micelles leading to longer polymers.

In order to highlight the crucial role played by our LC templates in determining the final morphology of the polymer nanostructures and in order to demonstrate that the spindle shape as well as the balled-up structures of PEDOT result from the *in situ* growth of polymers within mesophases, we first synthesized PEDOT polymers in bulk solutions by mixing EDOT and $FeCl_3$ (both at 0.1 M). As expected, under these conditions, in the absence of any mesophases, an aggregated network structure of PEDOT was obtained as shown in Fig. S5 (ESI†). The further incorporation of these bulk PEDOT polymers into the hexagonal mesophases, followed by an extraction step, produced highly aggregated polymer structures (Fig. S6, ESI†). Once again, neither spindle shaped objects, nor balled-up structures, were observed. This definitely proves that the morphology of PEDOT nanostructures results from the confinement of the reactive species into the mesophases and of course from further *in situ* polymerization. However, the influence of the architecture of the mesophases on the morphology of the polymer nanostructures is not well understood. Nevertheless, by varying the experimental conditions, in particular the geometry of the mesophases, the key parameters which control the polymer structure could be identified.

In order to check the eventual influence of the substrate (ZnSe) on the morphology of the PEDOT nanostructures and in order to characterize the twisted and balled up structures which we previously observed in the optical images (Fig. S4, ESI†), TEM and SEM experiments were carried out at different NaCl concentrations (0.1 M and 0.3 M). Once again and in good agreement with the previous observations of ZnSe, two kinds of nanostructures were observed on both carbon grids and aluminium substrates by both TEM and SEM techniques: (i) spindle-shaped objects and (ii) balled-up objects which appear as open vesicles. This result demonstrates that the deposition procedure and the nature of the substrate have no effect on the final morphology of the synthesized polymers. As already proposed, the kinetics of the polymerization process as well as the structure of the mesophases should have a direct impact on the size and the shape of the formed nanostructures. However for the moment, we have no clear explanation concerning the formation of the vesicles. Possibly, they could result from the lamellar packing of spindle-shaped PEDOT nanostructures.

As previously observed in the optical images (Fig. S4, ESI†) and as demonstrated by both SEM and TEM techniques, the open vesicle structures are predominant when PEDOT polymers are synthesized in mesophases in the presence of 0.1 M NaCl (Fig. 6), while the spindle shaped objects are predominant at higher salt concentration (0.3 M NaCl) (Fig. 7). The PEDOT vesicles obtained when polymers are synthesized in mesophases, at 0.1 M NaCl in the presence of both EDOT and $FeCl_3$ at 0.1 M, present a thickness of around 40 nm and a diameter of 1 μm as observed in SEM and TEM images (Fig. 6).

The size of spindle-shaped PEDOT nanostructures observed in Fig. 7 is in good agreement with AFM measurements (Fig. 5). Indeed, a mean length of 2 μm is found for the nanoobjects in Fig. 5. Nevertheless, one can note that in SEM images, these objects appear thinner than those observed by AFM.

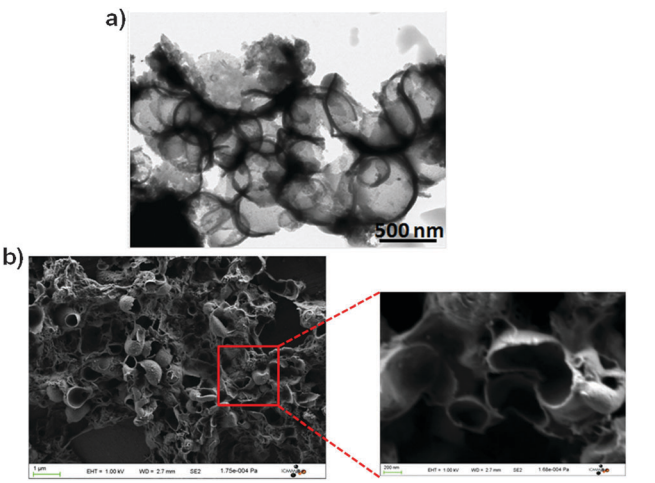

Fig. 6 TEM image of PEDOT open vesicles deposited onto the carbon grid (a) and the SEM image (with a zoom) of the same PEDOT vesicles deposited onto the aluminium substrate (b). In both cases, PEDOT polymers are synthesized in mesophases at 0.1 M NaCl in the presence of 0.1 M EDOT and 0.1 M $FeCl_3$.

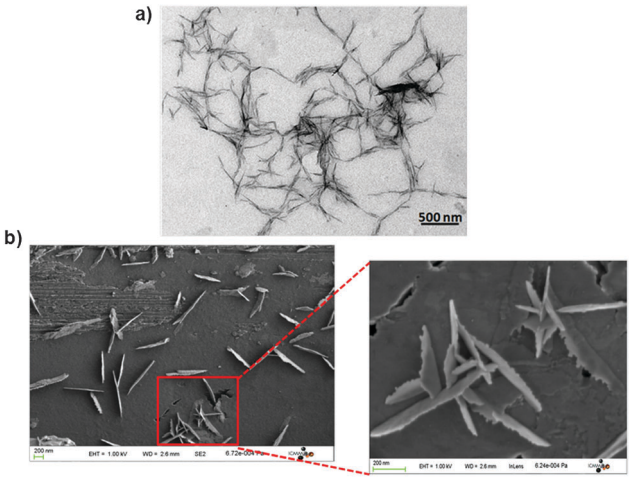

Fig. 7 TEM image of spindle-shaped PEDOT deposited onto carbon grid (a) and SEM image (with a zoom) of the same spindle shaped PEDOT deposited onto the aluminium substrate (b). In both cases, PEDOT polymers are synthesized in mesophases at 0.3 M NaCl in the presence of 0.1 M EDOT and 0.1 M $FeCl_3$.

Indeed, SEM images demonstrate the flatness of the spindle-shaped objects, the thickness of which is about a few nanometers. If we suppose that the objects observed by AFM and SEM are the same, the observed morphological difference could be due to the orientation of the spindle shaped nanostructures onto the different substrates. While the spindle-shaped nanostructures appear perpendicular to the aluminum substrate in SEM measurements, they remain more or less flattened on the ZnSe substrate in AFM experiments. This could be explained in terms of intermolecular interactions. Since PEDOT nanostructures are made of hydrophobic polymers, they should minimize their interaction with aluminium substrates since the latter are spontaneously covered in air by a thin hydrophilic surface layer made of aluminium oxide.

Thermal stability and conducting properties of PEDOT

Due to its excellent thermal stability and its high electrical conductivity, PEDOT polymer is one of the most extensively used conducting materials.[10] After extraction from mesophases, the thermal and electrical properties of our PEDOT polymers were then evaluated. The thermal stability of PEDOT polymers synthesized in mesophases at 0.1 M NaCl, in the presence of EDOT and $FeCl_3$ both at 0.1 M, was studied by thermogravimetry analysis (TGA) and differential scanning calorimetry (DSC) in a nitrogen environment (Fig. 8).

Fig. 8a depicts a TGA curve which enables the evaluation of the weight loss over time while the sample is heated at a constant rate. The TGA results show that PEDOT undergoes a continuous thermal degradation from 200 °C until a major decomposition occurs at around 550 °C. At 600 °C, only a small amount (15%) of an inert residue remains. Such a result is in agreement with earlier reports concerning PEDOT.[51] Indeed, it has been reported that at about 250 °C, the PEDOT weight decreases significantly and further, at higher temperatures

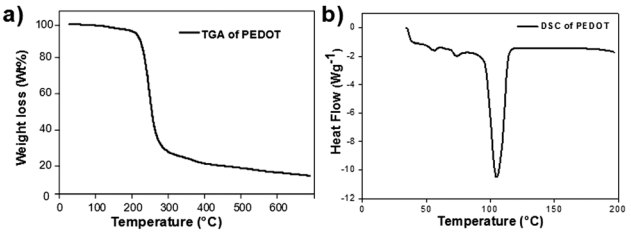

Fig. 8 TGA profile (a) and DSC profile (b) of solid PEDOT nanostructures after extraction from the mesophases. PEDOT polymers were synthesized in mesophases at 0.1 M NaCl in the presence of 0.1 M EDOT and 0.1 M $FeCl_3$.

around 350 °C, other fragments due to carbon oxidation are detected. In addition, PEDOT displays a decomposition pattern up to 550 °C with a weight loss of about 74 wt% at 300 °C and an additional 10 wt% loss at 550 °C. As a consequence, the PEDOT polymers synthesized in hexagonal mesophases are characterized by thermal stability which is as good as that of the PEDOT polymers described in the literature.

Our PEDOT can be considered to be thermally stable up to 200 °C. In DSC analysis, PEDOT extracted from mesophases was heated to about 200 °C. A sharp endothermic transition peak was observed at 105 °C (Fig. 8b). We can then definitely infer that our PEDOT polymers do not display any degradation up to 200 °C. In addition, the pure phase of PEDOT is obtained after extraction, thanks to our methodology.

The electrical conductivity of conjugated polymers depends significantly on their morphology, their microstructure and the number of counter ions that balance the positive doping charges carried by the conjugated polymer chains.[52] After extraction from mesophases, after dissolution into ethanol and after spread out by spin-coating onto the glass substrate, the electrical conductivity of the obtained dark blue colored PEDOT films was evaluated by using a four-point probe device. In the case of PEDOT thin films made up of polymers synthesized in mesophases at 0.1 M NaCl, in the presence of EDOT and $FeCl_3$ (both at 0.1 M), the average conductivity was evaluated to be 7×10^{-2} S cm^{-1}. This value is comparable with some conductivity values already reported in the literature for PEDOT[53–55] and remains higher than conductivity values of PEDOT nanostructures usually synthesized *via* oxidative polymerization in bulk solution.[56] Besides, the same PEDOT nanostructures obtained after extraction from mesophases were treated with $NOBF_4$ in acetonitrile and were then spin-coated onto the glass substrate forming, this time, transparent layers. The four probe measurements provided after doping a relatively high conductivity value up to 0.4 S cm^{-1}.

Conclusion

In the present study, we developed a simple, widely applicable, cost effective, one pot synthesis of PEDOT polymers at a submicron scale, in the confined geometry of oil-swollen tubes within a stable soft hexagonal matrix. Moreover, we showed that the PEDOT polymers prepared in mesophases can be easily

extracted from their confined media and are quite simply redispersed in alcohol solutions.

We demonstrated that the morphology of PEDOT nanostructures results first from the confinement of both EDOT (monomers) and the iron salt (oxidizing species) into the mesophases and second from further *in situ* polymerization. A detailed investigation of PEDOT structure after extraction from mesophases revealed the formation of two kinds of objects: spindle-like or vesicle-like morphologies, the ratio of which depends on the experimental conditions.

PEDOT polymers synthesized in the mesophases are characterized by a very good long-term stability in air in a humid environment. Besides, we demonstrated that the as-prepared PEDOT nanostructures possess good thermal stability and an electrical conductivity which are comparable with those of PEDOT polymers described in the literature. Conductivity of PEDOT nanostructures was also successfully improved from 10^{-2} to 0.4 S cm^{-1}, thanks to $NOBF_4$ doping.

Work is in due course in order to identify, thanks to the variation of mesophase geometry, the key parameters which control the growth kinetics as well as the polymer morphology. Our aim is the optimization of the preparation, within the mesophases, of conducting materials with controlled shapes and enhanced properties. Also, we aim to use ''softer'' alternative physico-chemical methodologies for synthesizing PEDOT nanostructures within mesophases. Experiments using photochemistry or, more originally, radiation chemistry are in due course.

Acknowledgements

We acknowledge the RBUCE program, the European Commission and the PRES UniverSud for a postdoctoral fellowship (Marie Curie Co-fund). We also thank Dr Jean-Michel Guigner (IMPMC, Université Pierre et Marie Curie, France) for Cryo-TEM experiment.

Notes and References

1 J. Kao, K. Thorkelsson, P. Bai, B. J. Rancatore and T. Xu, *Chem. Soc. Rev.*, 2013, **42**, 2654–2678.
2 M. Sarikaya, C. Tamerler, A. K. Y. Jen, K. Schulten and F. Baneyx, *Nat. Mater.*, 2003, **2**, 577–585.
3 J. D. Yuen, R. Menon, E. C. Nelson, E. B. Namdas, S. Cho, S. T. Hannahs, D. Moses and A. J. Heeger, *Nat. Mater.*, 2009, **8**, 572–575.
4 I. B. Martini, I. M. Craig, W. C. Molenkamp, H. Miyata, S. H. Tolbert and B. J. Schwartz, *Nat. Nanotechnol.*, 2007, **2**, 647–652.
5 F. Huang, Y. Zhang, M. S. Liu and A. K. Y. Jen, *Adv. Funct. Mater.*, 2009, **19**, 2457–2466.
6 P. A. Troshin, D. K. Susarova, Y. L. Moskvin, I. E. Kuznetsov, S. A. Ponomarenko, E. N. Myshkovskaya, K. A. Zakharcheva, A. A. Balakai, S. D. Babenko and V. F. Razumov, *Adv. Funct. Mater.*, 2010, **20**, 4351–4357.
7 H. Y. Chen, J. Hou, S. Zhang, Y. Liang, G. Yang, Y. Yang, L. Yu, Y. Wu and G. Li, *Nat. Photonics*, 2009, **3**, 649–653.
8 Y. Zhou, W. Huang, J. Liu, X. Zhu and D. Yan, *Adv. Mater.*, 2010, **22**, 4567–4590.
9 B. Winther-Jensen and K. I. West, *React. Funct. Polym.*, 2006, **66**, 479–483.
10 B. L. Groenendaal, F. Jonas, D. Freitag, H. Pielartzik and J. R. Reynolds, *Adv. Mater.*, 2000, **12**, 481–494.
11 A. Elschner, S. Kirchmeyer, W. Lovenich, U. Merker and K. Reuter, *PEDOT: Principles and Applications of an Intrinsically Conductive Polymer*, CRC Press, Taylor and Francis Group, 2010, vol. 1, pp. 41–63.
12 X. Wang, T. Ishwara, W. Gong, M. Campoy-Quiles, J. Nelson and D. D. C. Bradley, *Adv. Funct. Mater.*, 2012, **22**, 1454–1460.
13 P. A. Levermore, L. Chen, X. Wang, R. Das and D. D. C. Bradley, *Adv. Mater.*, 2007, **19**, 2379–2385.
14 Y. Lattach, F. Garnier and S. Remita, *ChemPhysChem*, 2012, **13**, 281–290.
15 M. Mumtaz, E. Ibarboure, C. Labrugére, E. Cloutet and H. Cramail, *Macromolecules*, 2008, **41**, 8964–8970.
16 J. L. Duvail, P. Retho, S. Garreau, G. Louarn, C. Godon and S. Demoustier-Champagne, *Synth. Met.*, 2002, **131**, 123–128.
17 S. G. Im, D. Kusters, W. Choi, S. H. Baxamusa, M. C. M. van de Sanden and K. K. Gleason, *ACS Nano*, 2008, **2**, 1959–1967.
18 W. Li, G. Zheng, Y. Yang, Z. W. Seh, N. Liu and Y. Cui, *Proc. Natl. Acad. Sci. U. S. A.*, 2013, **110**, 7148–7153.
19 L. Pan, G. Yu, D. Zhai, H. R. Lee, W. Zhao, N. Liu, W. H. Huiliang, C. K. Benjamin, T. Y. Shi, Y. Cui and Z. Bao, *Proc. Natl. Acad. Sci. U. S. A.*, 2012, **109**, 9287–9292.
20 L. Youssef, A. Deniset-Besseau, J.-M. Guigner and S. Remita, *Radiat. Phys. Chem.*, 2013, **82**, 44–53.
21 F. Goubard, P.-H. Aubert, K. Boukerma, E. Pauthe and C. Chevrot, *Chem. Commun.*, 2008, 3139–3140.
22 J. Kotz and S. Kosmella, *Curr. Opin. Colloid Interface Sci.*, 1999, **4**, 348–353.
23 B.-G. Kim, E. J. Jeong, J. W. Chung, S. Seo and B. K. J. Kim, *Nat. Mater.*, 2013, **12**, 659–664.
24 H. P. Hentze and E. W. Kale, *Curr. Opin. Colloid Interface Sci.*, 2003, **8**, 164–178.
25 J. F. Hulvat and S. I. Stupp, *Adv. Mater.*, 2004, **16**, 589–592.
26 H. Goto, *J. Mater. Chem.*, 2009, **19**, 4914–4921.
27 J. F. Hulvat and S. I. Stupp, *Angew. Chem., Int. Ed.*, 2003, **42**, 778–781.
28 G. Surendran, M. S. Tokumoto, E. Pena dos Santos, H. Remita, L. Ramos, P. J. Kooyman, C. V. Santilli, C. Bourgaux, P. Dieudonné and E. Prouzet, *Chem. Mater.*, 2005, **17**, 1505–1514.
29 F. Ksar, L. Ramos, B. Keita, L. Nadjo, P. Beaunier and H. Remita, *Chem. Mater.*, 2009, **21**, 3677–3683.
30 A. Lehoux, L. Ramos, P. Beaunier, D. B. Uribe, P. Dieudonné, F. Audonnet, A. Etcheberry, M. José-Yacaman and H. Remita, *Adv. Funct. Mater.*, 2012, **22**, 4900–4908.
31 E. Pena dos Santos, M. S. Tokumoto, G. Surendran, H. Remita, C. Bourgaux, P. Dieudonné, P. Prouzet and L. Ramos, *Langmuir*, 2005, **21**, 4362–4369.
32 L. Ramos and P. Fabre, *Langmuir*, 1997, **13**, 682–686.

33 G. Surendran, G. Apostolescu, M. Tokumoto, E. Prouzet, L. Ramos, P. Beaunier, P. J. Kooyman, A. Etcheberry and H. Remita, *Small*, 2005, **1**, 964–967.
34 F. Ksar, G. Surendran, L. Ramos, B. Keita, L. Nadjo, E. Prouzet, P. Beaunier, A. Hagège, F. Audonnet and H. Remita, *Chem. Mater.*, 2009, **21**, 1612–1617.
35 P. F. Siril, L. Ramos, P. Beaunier, P. Archirel, A. Etcheberry and H. Remita, *Chem. Mater.*, 2009, **21**, 5170–5175.
36 H. P. Hentze and E. W. Kaler, *Chem. Mater.*, 2003, **15**, 708–713.
37 T. M. Dellinger and P. V. Braun, *Chem. Mater.*, 2004, **16**, 2201–2207.
38 A. Dazzi, R. Prazeres, F. Glotin and J. M. Ortega, *Opt. Lett.*, 2005, **30**, 2388–2390.
39 C. Policar, J. B. Waern, M.-A. Plamont, S. Clède, C. Mayet, R. Prazeres, J.-M. Ortega, A. Vessières and A. Dazzi, *Angew. Chem., Int. Ed.*, 2011, **50**, 860–864.
40 A. Dazzi, C. B. Prater, Q. Hu, D. B. Chase, J. F. Rabolt and C. Marcott, *Appl. Spectrosc.*, 2012, **66**, 1365–1384.
41 A. Dazzi, F. Glotin and R. Carminati, *Appl. Phys.*, 2010, **107**, 124519–124522.
42 J. C. Loudet, P. Barois and P. Poulin, *Nature*, 2000, **407**, 611–613.
43 C. Kvarnström, H. Neugbauer, S. Blomquist, H. J. Ahonen, J. Kankare and A. Ivaska, *Electrochim. Acta*, 1999, **44**, 2739–2750.
44 J. W. Choi, M. G. Han, S. G. Oh and S. S. Im, *Synth. Met.*, 2004, **141**, 293–299.
45 M. Lapkowski and A. Proń, *Synth. Met.*, 2000, **110**, 79–83.
46 A. Laforgue and L. Robitaille, *Macromolecules*, 2010, **43**, 4194–4200.
47 S. Garreau, J. L. Duvail and G. Louarn, *Synth. Met.*, 2002, **125**, 325–329.
48 C. Prater, K. Kjoller, D. Cook, R. Shetty, G. Meyers, C. Reinhardt, J. Felts, W. King, K. Vodopyanov and A. Dazzi, *Microsc. Anal.*, 2010, 5–8.
49 J. R. Felts, K. Kjoller, M. Lo, C. B. Prater and W. P. King, *ACS Nano*, 2012, **6**, 8015–8021.
50 M. Lapkowski and A. Proń, *Synth. Met.*, 2000, **110**, 79–83.
51 J. S. Kim, F. Cacialli, R. H. Friend, R. Daik and W. J. Feast, *Synth. Met.*, 1999, **102**, 1065–1066.
52 X. Crispin, S. Marciniak, W. Osikowicz, G. Zotti, A. Denier van der Gon, W. F. Louwet, M. Fahlman, L. F. Groenendaal, D. Schryver and W. R. Salaneck, *J. Polym. Sci., Part B: Polym. Phys.*, 2003, **41**, 2561–2583.
53 B. H. Jones, K.-Y. Cheng, R. J. Holmes and T. P. Lodge, *Macromolecules*, 2012, **45**, 599–601.
54 S. E. Nair, E. Hsiao and S. H. Kim, *Chem. Mater*, 2009, **21**, 115–121.
55 K. E. Aasmundtveit, E. J. Samuelsen, L. A. A. Pettersson, O. Inganäs, T. Johansson and R. Feidenhans, *Synth. Met.*, 1999, **101**, 561–564.
56 Y.-H. Ha, N. Nikolov, S.-K. Pollack, J. Mastrangelo, B.-D. Martin and R. Shashidhar, *Adv. Funct. Mater.*, 2004, **14**, 615–622.